Fractal geometry of nature (bone) may inspire medical devices shape

Salvatore Longoni[1] & Matteo Sartori[1]

[1]*S. Apollonia Dental Center, R&D Department, Lazzate (MB), Italy*

These authors contributed equally to this work

Medical devices, as orthopaedics prostheses and dental implants, have been designed over years on the strength of mechanical, clinical and biological indications. This sequence is the commonly accepted cognitive and research process: adapting the device to the surrounding environment (host tissue). Inverting this traditional logical approach, we started from bone microarchitecture analysis. Here we show that a unique geometric rule seems to underlie different morphologic and functional aspects of human jaw bone tissue: fractal properties of white trabeculae in low quality bone are similar to fractal properties of black spaces in high quality bone and *vice versa*. These data inspired the fractal bone quality classification and they were the starting point for reverse engineering to design specific dental implants threads. We introduce a new philosophy: bone decoding and with these data devices encoding. In the future, the method will be implemented for the analysis of other human or animal tissues in order to project medical devices and biomaterials with a microarchitecture driven by nature.

Nowadays patients that loose function and aesthetic after disease or trauma undergo surgical procedures to place a medical device to improve their quality of life. Over the last 30 years, efforts have been made in attempt to enhance the performance of devices in relation to type of materials, biomechanical design and surface interaction with host tissue[1].

The evolution of orthopaedic and dental devices has advanced on various levels. As concerns the materials, by far the most commonly used material on an international scale is titanium and its alloys. The majority of the devices produced have a cylindrical-conical morphology with or without threads or similar means for anchorage. Devices morphology guarantees primary stability and enables the osseointegration process to develop. During and after this process, device morphology determines the distribution of the functional loads in the surrounding bone[2-11]. The surface of devices affects the dynamics of osseointegration in terms of quantity, quality and duration. First devices were smooth, but a great variety of modified surfaces subsequently became available on the market, obtained by adding or subtracting material and/or bioactive components at micrometric and/or nanometric level. These surfaces increase the wettability attracting the organic fluids contained in bone, thereby reducing the time for achieving osseointegration and creating a greater contact area at bone-device interface[12-15].

The average duration of orthopaedics and dental devices is roughly 10-15 years before the necessity of revision: this depends largely on patient's health, bone quality, functional load, device morphology and surface[16-20]. They have different macrogeometry (shape) and surface depending on manufacturer and they can be selected by clinicians in relation only to their dimensions (size) but not in relation to bone quality. It must be noted here that bone quality has been classified by other Authors in 3 or 4 types based on cortical and trabecular bone quantity and density[4,21-23].

Recognised orthopaedic and dental devices have been designed, manufactured and perfected over years on the strength of mechanical, clinical and biological indications. This sequence is the commonly accepted cognitive and research process: adapting the device to the surrounding environment (bone). All this knowledge represents the current state of art, but the important role of devices shape in relation to bone

microarchitecture[3,4,12], made us researching morphological solutions to improve quality and duration of their osseointegration.

We started inverting the traditional logical approach: the first step should be the analysis of bone natural geometry, in order to design new shapes for medical devices. In this way, we introduce a new philosophy: bone decoding and with these data devices encoding (Supplementary Fig. 1).

Bone Decoding: RQA fractal breakdown

We collected forty human jaw bone cylindrical specimens (diameter 2.5 mm and length 8 mm) during standard surgical protocol for dental implants insertion and the histologist prepared them for micro-X-ray[24]. The digital images obtained were processed with a specific software conceived by the Authors: the algorithm was named Recursive Quadrants Analysis (RQA) (Supplementary Fig. 2). The RQA algorithm is a particular application of what, in the software technology sector, is called Quadtree[25-28]: this is a data tree structure in which each node has four branches. RQA algorithm is a fractal scale-independent method[29] that can be applied to images of tissues at different level of magnification. The software analyzed the trabecular structure of bone micro-X-rays evaluating both white areas (bone trabeculae) or black areas (spaces containing bone marrow). RQA algorithm had as input the original digital micro-X-ray image represented as a pixel matrix, as each pixel is characterized by its colour (white or black). After image size calibration, a square region of interest (ROI: 512*512 pixels) was selected. The analysis of ROI was based on a recursive scale independent subdivision of white or black areas using square quadrants: quadrant base iterative binarization. For each recursion level the dimension of the quadrants was a submultiple of the previous level. In particular, ROI was recursively split into four quadrants when the percentage of white pixels was below a higher threshold (e.g. 95%) and above a

lower threshold (e.g. 2%); otherwise all pixels were set to white if the white-pixel percentage was above said higher threshold or set to black if the percentage was below said lower threshold. Starting from whole ROI, said steps of testing against the thresholds, splitting into quadrants and colour setting were repeatedly carried out of each created quadrants, until newly created quadrants were small enough size (e.g. 1 pixels): we obtained 10 recursion levels.

At the end of the reiterations of RQA algorithm, every pixel of the original picture was part of either a black or a white quadrant. In this way, the RQA was capable to remap the original image in a bunch of quadrants of various sizes. The method thus led to the breakdown of the image into increasingly small quadrants, the dimensions of which were inversely proportional to the recursion level used to obtain them (Fig. 1a). In particular, dimension of ROI, percentages and colours of RQA algorithm may be varied in software settings in relation to characteristics of images and tissues analyzed.

Then, two graphs were automatically plotted: white areas graph and black areas graph. The graphs correlated the recursion levels (abscissa axis) with the percent coverage assured by the quadrants belonging to each level (ordinate axis). Percentages were in relation to whole ROI (100%). The peak of the curve (white or black) corresponded to the Maximum Recursion Level: W-MRL (White Maximum Recursion Level) and B-MRL (Black Maximum Recursion Level). Quadrants belonging to W-MRL and B-MRL gave the best percent coverage of the analyzed area (white or black) with RQA analysis: W%-MRL and B%-MRL (Fig.1 b).

This recursive method took into account the amounts of the colours (white or black), their spatial distribution, and consequently distinguished automatically between images with different texture, even though they may contain similar amounts of white and black. Moreover, it provided more information than the classic Fractal-Dimension

approach based on the box-counting method, which is only capable of providing information relating to the unevenness of the image analysed[30-37]. Infact, with RQA algorithm we measured: the white areas occupied by the trabeculae (TWA: Total White Area, percent white coverage corresponding to classic Bone Volume percentage[38,39]) and the black areas between the trabeculae (TBA: Total Black Area, percent black coverage), the number of white and black quadrants obtained at each recursion, the percent weight of the quadrants belonging to each recursion level in the composition of whole image, W-MRL, B-MRL, W%-MRL and B%-MRL values. Since each recursion level had a specific dimension in relation to ROI and image calibration, the W-MRL and B-MRL were also indicators of trabecular and black spaces size.

Bone Decoding: Fractal Bone Quality Classification

Categorical variables were described reporting absolute and percentage frequencies, while quantitative ones by mean and standard deviation (s.d.). All statistical test were performed with an alpha level of 0.05, except for contrasts.

In the 40 images examined, we investigated the correlation between white area occupied by trabeculae (TWA: Total White Area) and W%-MRL (percent area covered by quadrants belonging to W-MRL). The Pearson correlation coefficient showed a high positive correlation between these variables and this correlation was statistically significant: $\rho = 0.95145$, $p<0.0001$- two tailed. As consequence, W-MRL might be considered the fractal basic module of trabeculae in human jaw bone images analyzed with RQA algorithm (Fig. 2a).

Moreover, the ANOVA model was applied to evaluate the association of TWA and W-MRL among the 40 specimens. In particular, ranging from low density to high density bone (i.e. from min TWA to max TWA) W-MRL values were respectively 5, 4 and 3. Couple TWA comparisons were computed using the alpha level adjusted by the

Bonferroni correction (α=0.017), basing on the total of 3 comparisons planned. Results from the ANOVA model showed that the differences between the 3 means of TWA (mean-TWA) calculated for specimens with W-MRL 5, W-MRL 4 and W-MRL 3 were statistically significant ($F= 13.89$ $p<0.0001$). All the contrasts, evaluated with an alpha level of 0.017, resulted statistically significant: in particular W-MRL 3 vs W-MRL 4 (respectively -n=8, 20%- 60.985±15.218% vs -n=23, 57.5%- 41.563±16.386%, $p=0.0023$), W-MRL 3 vs W-MRL 5 (respectively -n=8, 20%- 60.985±15.218% vs -n=9, 22.5%- 23.908±5.296%, $p<0.0001$) and W-MRL 4 vs W-MRL 5 (respectively -n=23, 57.5%- 41.563±16.386% vs -n=9, 22.5%- 23.908±5.296%, $p=0.0037$).

In this way, with RQA algorithm running for white areas, we provided a fractal based bone quality classification. In particular, we identified 3 different classes of human jaw bone microarchitecture that are characterized by specific mean-TWA±SD and W-MRL values: low quality bone (mean-TWA 23.908± 5.296% and W-MRL 5), medium quality bone (mean-TWA 41.563± 16.386% and W-MRL 4) and high quality bone (mean-TWA 60.985± 15.218% and W-MRL 3) (Fig. 2b).

The same analyses were performed for black areas (hollows containing bone marrow). We analyzed the correlation between black area (TBA: Total Black Area) and B%-MRL (percent area covered by quadrants belonging to B-MRL). The Pearson correlation coefficient showed a high positive correlation between these variables and this correlation was statistically significant: $\rho = 0.89617$, $p<0.0001$- two tailed. As consequence, B-MRL might be considered the fractal basic module of spaces between trabeculae in human jaw bone images analyzed with RQA algorithm (Fig. 3a).

ANOVA model was also applied to assess the association between TBA and B-MRL among the 40 specimens. In particular, ranging from low density to high density bone (i.e. from max TBA to min TBA) B-MRL values were respectively 2, 3, 4 and 5.

In this case, as 6 TBA comparisons were planned, the adjusted α level was 0.0083 (Bonferroni correction). Results from the ANOVA model showed that the 4 means of TBA (mean-TBA) calculated for specimens with B-MRL 2, B-MRL 3, B-MRL 4 and B-MRL 5 were statistically different ($F=8.93$ $p<0.0001$). In particular the following contrasts resulted statistically significant with an adjusted alpha level of 0.0083: B-MRL 2 vs B-MRL 4 (respectively -n=3, 7.5%- 83.39±2.82% vs -n=20, 50%- 54.87±16.02%, $p=0.0034$), B-MRL 2 vs B-MRL 5 (respectively -n=3, 7.5%- 83.39±2.82% vs -n=5, 12.5%- 35.68±18.74%, $p<0.0001$) and B-MRL 3 vs B-MRL 5 (respectively -n=12, 30%- 67.92±11.61 vs -n=5, 12.5%- 35.68±18.74%, $p=0.0002$) (Fig. 3b). These data (derived from black spaces analysis) gave additional morphological information to the fractal based bone quality classification, derived from white areas analysis. In particular, starting from the breakdown of the original image into 10 recursion levels, we show that RQA fractal properties of white trabeculae in low quality bone (W-MRL 5) are similar to RQA fractal properties of black spaces in high quality bone (B-MRL 4-5) and *vice versa* RQA fractal properties of white trabeculae in high quality bone (W-MRL 3) are similar to RQA fractal properties of black spaces in low quality bone (B-MRL 2 and 3). Moreover, in medium quality bone RQA fractal properties of white trabeculae and black spaces are balanced. In conclusion, a unique geometric rule seems to underlie different morphologic and functional aspects of human jaw bone tissue.

Bone Decoding: Island detection

The quadrants generated at each stage of the iterative binarization were particularly well suited for determining clusters in a simple and economical way. Thus, the image broken down with the RQA algorithm was further analysed to identify the number and structure of its basic components, that were named "islands". These islands were clusters of quadrants that were grouped together on the basis of their size and position according to a precise spatial hierarchy based on the assessment of the quadrants dimensions and

adjacency relationships. The procedure was performed automatically by the software and it was conducted both for the colour white and for the colour black (Supplementary Fig. 3 and Supplementary Fig. 4). The procedure began with the larger-sized quadrants, which represented the central nucleus of each island. The adjacent quadrants of smaller dimensions (higher recursion levels) lying along their sides were associated with the larger quadrant and considered as belonging to the same island. When a given quadrant came into contact with the island on a level with a corner (i.e. a contact that was not linear along its side) this meant that said quadrant belonged to another island. The larger-sized quadrants thus represented the load-bearing framework of each island, and they were surrounded by quadrants of progressively decreasing dimensions. Then, the quadrants constituting the single islands were counted and their dimensions were recorded. Moreover, the number and the probability of the adjacencies between the different quadrants and the different recursion levels in the islands were calculated. Values of all islands were averaged.

Devices Encoding: artificial fractal island generation with Quadrant Fall algorithm

The data obtained by the Islands algorithm were used to generate artificial fractal islands lying on the horizontal X axis on a probabilistic basis. The procedure was performed automatically by the software (Quadrant Fall algorithm) and it was conducted both for the colour white and for the colour black (Supplementary Fig. 5). The artificial islands were generated by dropping onto X axis first the larger-sized quadrants and then the smaller-sized quadrants, complying with quadrants number and the probability of adjacency derived from the average of quadrants number and of islands adjacencies that constitute the original image. In particular, if there was more than one position with the same probability of being the best position in relation to adjacency, then a random choice among said more than one position was made. Thus

artificial islands had geometrical characteristics compatible with the islands on the original source image, in terms of both number, dimension of quadrants and adjacencies between them. In particular, the side of the artificial island placed onto X axis was flat and the other sides had a fragmented geometric shape (fractal).

As random variables have been implied, Quadrant Fall algorithm was repeated a high number of times (e.g. 100 times) so that 100 different results were generated. For each result a consistency value was obtained from the formula C(%)=100-100 SUM(J)/SUM(K) wherein SUM (J) was the sum of the adjacencies of the fractal artificial island obtained by Quadrant Fall algorithm, and SUM (K) was the sum of the adjacencies of source image islands. A greater C (%) implied a better consistency.

Devices Encoding: dental implants thread design.

The artificial white and black fractal islands were the starting point for reverse engineering: device encoding. They were used to conceive and design dental implants thread in relation to the macro- and micro-geometry of host bone tissue. The aim was to mimic jaw bone fractal properties reproducing the specific morphologic dimensions, position and proportion between white trabeculae and black spaces according to RQA fractal bone quality classification. Restated we designed implants thread to maximize bone implant contact.

We analyzed three different bone qualities images: high quality bone, medium quality bone and low quality bone. For each bone quality, the corresponding artificial white and black islands with best consistency were placed along Y axis: each white fractal island was followed by a black fractal island. Artificial fractal black islands were placed with their flat base onto the Y axis and exposing their external apex to one side. Artificial white islands were placed with their flat base onto the Y axis and exposing their external apex to the opposite side (Fig. 4a, 4b, 5a, 5b, 6a, 6b). Then, a line was

designed following the external limit of the artificial fractal highlands that have been arranged: it was the thread outline.

The 3 threads obtained (high quality bone thread, medium quality bone thread and low quality bone thread) were different in terms of shape, pitch, depth in order to achieve an optimal filling of the intra-trabecular spaces enhancing bone-implant contact (Fig. 4c, 5c, 6c).

The process described may be used either to design a customized dental implant starting from a single bone image or to design implants with average characteristics according to bone quality classification, which can thus be tailored to the morphological features of the bone quality class concerned.

Current knowledge and technological opportunities allow us to explore nature rules. The RQA fractal analysis disclosed the morphological and geometric relationship between white trabeculae and black spaces: W-MRL values of low quality bone trabeculae are similar to B-MRL values of high quality bone black spaces and *vice versa*. In medium quality bone W-MRL and B-MRL values are balanced. This efficient natural project inspired the fractal bone quality classification and provided the key elements (artificial white and black fractal islands) to design specific dental implants threads (Supplementary Fig. 1). In the future, the method presented will be implemented and developed for the analysis of other human or animal tissues in order to project medical devices and biomaterials with a microarchitecture driven by nature.

1. Huebsch, N.& Mooney, D.J. Inspiration and application in the evolution of biomaterials. *Nature* **462**,426-432 (2009).

2. Eser, A., Tonuk, E., Akca, K. & Cehreli, M.C.. Predicting time-dependent remodeling of bone around immediately loaded dental implants with different designs. *Med. Eng. Phys.* **32,** 22-31 (2010).

3. Abuhussein, H., Pagni, G., Rebaudi, A. & Wang, H.L. The effect of thread pattern upon implant osseointegration. *Clin. Oral Implants Res.* **21,** 129-136 (2010).

4. Misch, C.E. *Contemporary Implant Dentistry*. 3rd edition, Mosby Elsevier, St. Louis, MO, USA (2008).

5. Petrie, C.S. & Williams, J.L. Comparative evaluation of implant designs: influence of diameter, length, and taper on strains in the alveolar crest. A three-dimensional finite-element analysis. *Clin Oral Implants Res.* **16,** 486-494 (2005).

6. Traini, T., Degidi, M., Strocchi, R., Caputi, S. & Piattelli A. Collagen fiber orientation near dental implants in human bone: do their organization reflect differences in loading? *J. Biomed. Mater. Res. B Appl. Biomater.* **74,** 538-546 (2005).

7. Steigenga, J.T., al-Shammari, K.F., Nociti, F.H., Misch, C.E. & Wang, H.L. Dental implant design and its relationship to long-term implant success. *Implant Dent.* **12,** 306-317 (2003).

8. Cruz, M., Wassall, T., Toledo, E.M., Barra, L.P. & Lemonge, A.C. Three-dimensional finite element stress analysis of a cuneiform-geometry implant. *Int. J. Oral Maxillofac. Implants.* **18,** 675-684 (2003).

9. Tada, S., Stegaroiu, R., Kitamura, E., Miyakawa, O. & Kusakari, H. Influence of implant design and bone quality on stress/strain distribution in bone around implants: a 3-dimensional finite element analysis. *Int. J. Oral Maxillofac. Implants.* **18,** 357-368 (2003).

10. Chun, H.J. et al. Evaluation of design parameters of osseointegrated dental implants using finite element analysis. *J. Oral Rehabil.* **29,** 565-574 (2002).

11. Patra, A.K., DePaolo, J.M., D'Souza, K.S., DeTolla, D. & Meenaghan, M.A. Guidelines for analysis and redesign of dental implants. *Implant Dent.* **7,** 355-368 (1998).

12. Davies, JE. *Bone Engineering.* Em squared incorporated, Toronto, Canada (2000).

13. Wennerberg, A. & Albrektsson, T. Effects of titanium surface topography on bone integration: a systematic review. *Clin. Oral Implants Res.* **20,** Suppl 4, 172-184 (2009).

14. Zhao, G. et al. Osteoblast-like cells are sensitive to submicron-scale surface structure. *Clin. Oral Implants Res.* **17,** 258-264 (2006).

15. Cochran, D.L., Schenk, R.K., Lussi, A., Higginbottom, F.L. & Buser, D. Bone response to unloaded and loaded titanium implants with a sandblasted and acid-etched surface: a histometric study in the canine mandible. *J. Biomed. Mater. Res.* **40,** 1-11 (1998).

16. Lambert, F.E., Weber, H.P., Susarla, S.M., Belser, U.C. & Gallucci, G.O. Descriptive analysis of implant and prosthodontic survival rates with fixed implant-supported rehabilitations in the edentulous maxilla. *J. Periodontol.* **80,** 1220-1230 (2009).

17. Jemt, T. & Johansson, J. Implant treatment in the edentulous maxillae: a 15-year follow-up study on 76 consecutive patients provided with fixed prostheses. *Clin Implant Dent. Relat. Res.* **8,** 61-9 (2006).

18. Astrand, P., Ahlqvist, J., Gunne, J. & Nilson, H. Implant treatment of patients with edentulous jaws: a 20-year follow-up. *Clin. Implant Dent. Relat. Res.* **10,** 207-217 (2008).

19. Sayeed, S.A, Trousdale, R.T., Barnes, S.A., Kaufman, K.R. & Pagnano, M.W. Joint arthroplasty within 10 years after primary charnley total hip arthroplasty. *Am. J. Orthop. (Belle Mead NJ).* **38,** 141-143 (2009).

20. Kurtz, S. et al. Prevalence of primary and revision total hip and knee arthroplasty in the United States from 1990 through 2002. *J. Bone Joint Surg. Am.* **87,** 1487-1497 (2005).

21. Trisi, P. & Rao, W. Bone classification: clinical-histomorphometric comparison. *Clin. Oral Implants Res.* **10,** 1–7 (1999).

22. Friberg, B., Sennerby, L., Roos, J. & Lekholm, U. Identification of bone quality in conjunction with insertion of titanium implants. A pilot study in jaw autopsy specimens. *Clin. Oral Implants Res.* **6,** 213-219 (1995).

23. Lekholm, U. & Zarb, G.A. *Patient selection and preparation.* In: Brånemark, P.-I., Zarb, G.A., Albrektsson, T., eds. *Tissue Integrated Prostheses: Osseointegration in Clinical Dentistry,* 199–209. Quintessence Publ Co., Chicago (1985).

24. Zaffe, D., Bertoldi, C., Palumbo, C. & Consolo, U. Morphofunctional and clinical study on mandibular alveolar distraction osteogenesis *Clin. Oral Implants Res.* **13,** 550–557 (2002).

25. Sankar, D. & Thomas, T. A new fast fractal modeling approach for the detection of microcalcifications in mammograms. *J. Digit. Imaging.* **Jul 18.** [Epub ahead of print] (2009).

26. Chen, Y.T. et al. The image feature analysis for microscopic thyroid tissue classification. *Conf. Proc. IEEE Eng. Med. Biol. Soc.* **2008,** 4059-4062 (2008).

27. Wang, L., Bhalerao, A. & Wilson, R. Analysis of retinal vasculature using a multiresolution Hermite model. *IEEE Trans. Med. Imaging.* **26,** 137-152 (2007).

28. Finkel R.A. & Bentley JL. Quad Trees a data structure for retrieval on composite keys. *Acta Informatica* **4,** 1-9 (1974).

29. Mandelbrot, B. *The Fractal Geometry of Nature.* W. H. Freeman & Co, NewYork, USA. (1982).

30. Hua, Y., Nackaerts, O., Duyck, J., Maes, F. & Jacobs R. Bone quality assessment based on cone beam computed tomography imaging. *Clin. Oral Implants Res.* **20,** 767-771 (2009).

31. Veltri, M., Balleri, P. & Ferrari M. Damping factor for monitoring the bone interface at dental implants. *Clin. Oral Implants Res.* **18,** 738-742 (2007).

32. Yasar, F. & Akgünlü, F. Fractal dimension and lacunarity analysis of dental radiographs. *Dentomaxillofac. Radiol.* **34,** 261-267 (2005).

33. Dougherty, G. & Henebry, G.M. Lacunarity analysis of spatial pattern in CT images of vertebral trabecular bone for assessing osteoporosis. *Med. Eng. Phys.* **24,** 129-138 (2002).

34. Fazzalari, N. L. & Parkinson, I.H. . Fractal properties of cancellous bone of the iliac crest in vertebral crush fracture. *Bone* **23,** 53–57 (1998).

35. Chappard, D., Grizon, F., Brechet, I., Baslé, M.F. & Rebel, A. Evolution of the bone-titanium interface on implants coated/noncoated with xenogeneic bone particles: quantitative microscopic analysis. *J. Biomed. Mater. Res.* **32,** 175-180 (1996).
36. Wilding, R.J. et al. The use of fractal analysis to reveal remodelling in human alveolar bone following the placement of dental implants. *Arch Oral Biol.* **40,** 61-72 (1995).
37. Oshida, Y., Hashem, A., Nishihara, T. & Yapchulay, M.V. Fractal dimension analysis of mandibular bones: toward a morphological compatibility of implants. *Biomed. Mater. Eng.* **4,** 397-407 (1994).
38. Norton, M.R. & Gamble C. Bone classification: an objective scale of bone density using the computerized tomography scan. *Clin. Oral Implants Res.* **12,** 79-84 (2001).
39. Thomsen, J.S., Ebbesen, E.N. & Mosekilde, L. Relationships between static histomorphometry and bone strength measurements in human iliac crest bone biopsies. *Bone* **22,** 153-163 (1998).

Supplementary Information accompanies the paper on **www.nature.com/nature**.

Acknowledgements We acknowledge Dr. F. Orsini Responsible for Statistical Planning in OPIS S.r.l. (Desio, MB, ITALY) for her support and statistical analysis; Ing. D. Vitulli for his support and software engineering.

Authors' Contributions S.L. and M.S. conceived the study, the software and wrote the manuscript.

Author Information Correspondence and requests for materials should be addressed to S.L. (salvatorelongoni@sapol.it).

Figure 1 Fractal bone decoding with Recursive Quadrants Analysis. a, A square region of interest (512*512 pixels) of the source bone image is analyzed with the recursive quandrants based algorithm RQA. Analysis is performed for both white trabeculae and black spaces. b, White trabeculae graph (blue line) and black spaces graph (red line) correlate the recursion levels (abscissa axis) with the percent coverage assured by the quadrants belonging to each level (ordinate axis). The peak of the curves corresponds to the Maximum Recursion Level: W-MRL (White Maximum Recursion Level) and B-MRL (Black Maximum Recursion Level). Quadrants belonging to W-MRL and B-MRL give the best coverage of the analyzed area (white or black) with RQA analysis : W%-MRL and B%-MRL.

Figure 2 Fractal bone quality classification: white analysis. a, High positive correlation between Total White Area (TWA) occupied by trabeculae and percent area covered by quadrants belonging to W-MRL (W%-MRL) b, RQA algorithm running for white areas and ANOVA identify 3 different classes of human jaw bone microarchitecture that are characterized by specific mean-TWA±SD and W-MRL values: low quality bone, medium quality bone and high quality bone. Yellow points indicate mean and error bars indicate s.d.

Figure 3 Fractal bone quality classification: black analysis. a, High positive correlation between Total Black Area (TBA) of spaces containg bone marrow and percent area covered by quadrants belonging to B-MRL (B%-MRL) b, RQA algorithm running for black areas and ANOVA identify 4 different classes that are characterized by specific mean-TBA±SD and B-MRL values. RQA fractal properties of white trabeculae in low quality bone (W-MRL 5) (Fig. 2b) are similar to RQA fractal properties of black spaces in high quality bone (B-MRL 4-5) and *vice versa* RQA fractal properties of white trabeculae in high quality

bone (W-MRL 3) are similar to RQA fractal properties of black spaces in low quality bone (B-MRL 2 and 3). Yellow points indicate mean and error bars indicate s.d.

Figure 4 Device encoding: high quality bone dental implant. a, High quality bone image analyzed with RQA algorithm: bone marrow spaces in red and bone trabeculae in yellow. b, Artificial black (red) and white (yellow) fractal island were paced along Y axis obtaining the outline of high quality bone dental implant thread. c, 3d design of high quality bone dental implant thread.

Figure 5 Device encoding: medium quality bone dental implant. a, Medium quality bone image analyzed with RQA algorithm: bone marrow spaces in red and bone trabeculae in yellow. b, Artificial black (red) and white (yellow) fractal island were paced along Y axis obtaining the outline of medium quality bone dental implant thread. **c,** 3d design of medium quality bone dental implant thread.

Figure 6 Device encoding: low quality bone dental implant. a, Low quality bone image analyzed with RQA algorithm: bone marrow spaces in red and bone trabeculae in yellow. b, Artificial black (red) and white (yellow) fractal island were paced along Y axis obtaining the outline of low quality bone dental implant thread. **c,** 3d design of low quality bone dental implant thread.

a

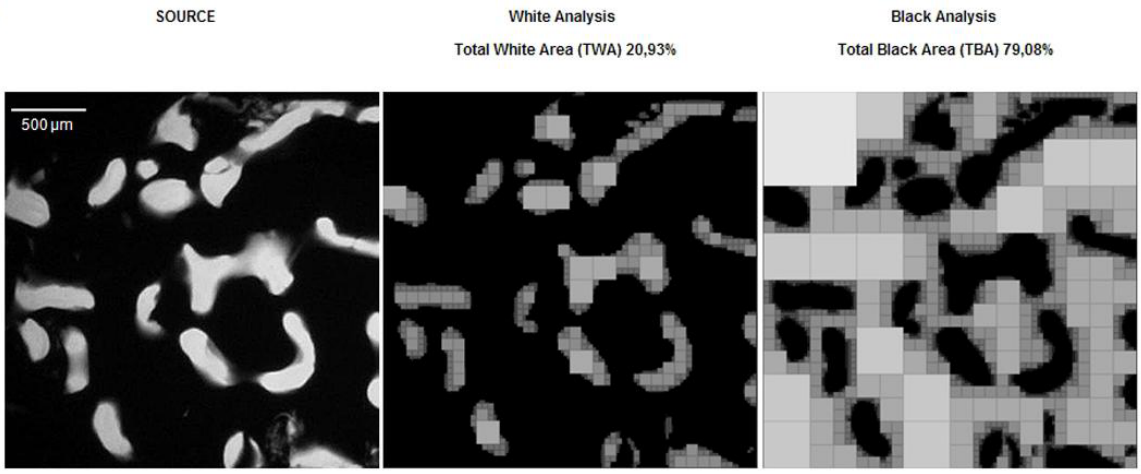
SOURCE
White Analysis
Total White Area (TWA) 20,93%
Black Analysis
Total Black Area (TBA) 79,08%
500 µm

b

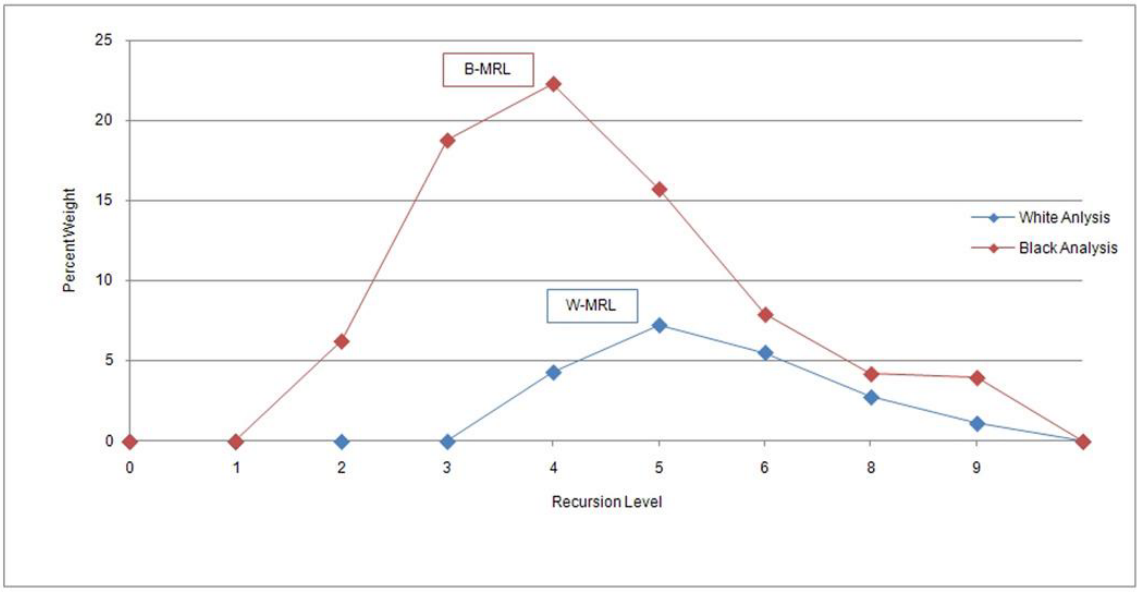
B-MRL
W-MRL
White Anlysis
Black Analysis
PercentWeight
Recursion Level
0
5
10
15
20
25
0
1
2
3
4
5
6
8
9

a

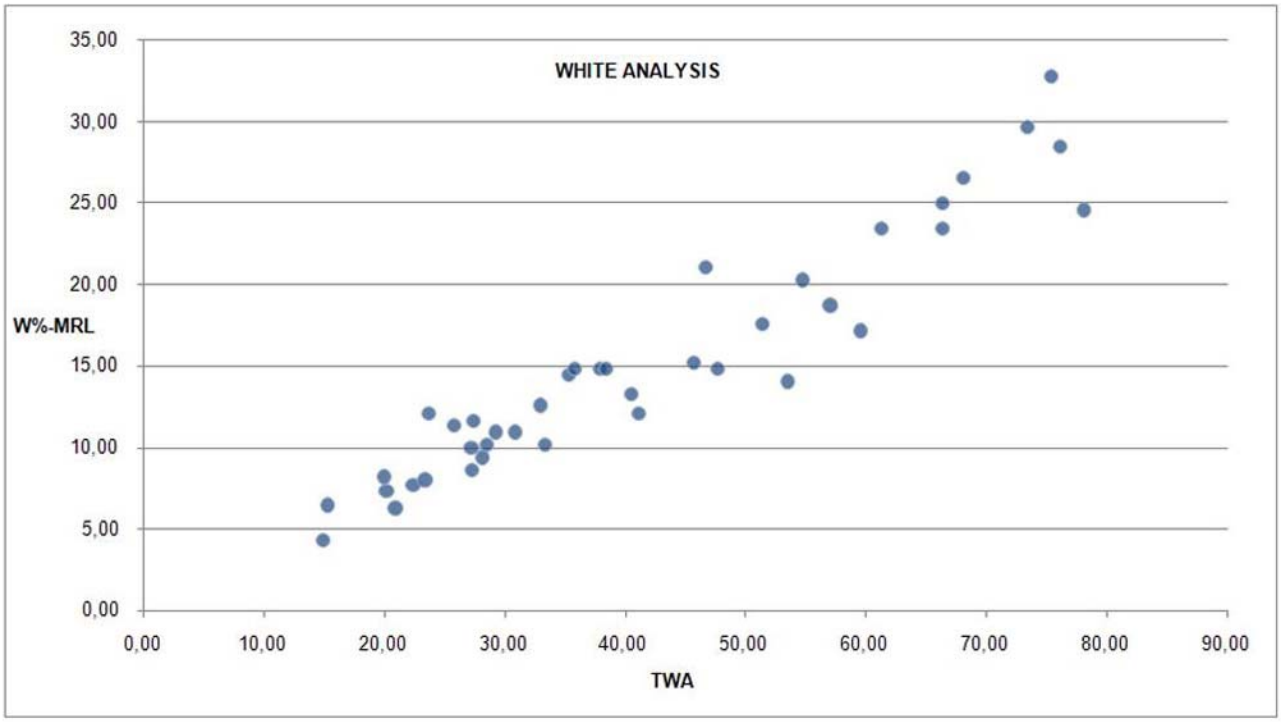
WHITE ANALYSIS
W%-MRL
TWA
35,00
30,00
25,00
20,00
15,00
10,00
5,00
0,00
0,00
10,00
20,00
30,00
40,00
50,00
60,00
70,00
80,00
90,00

b

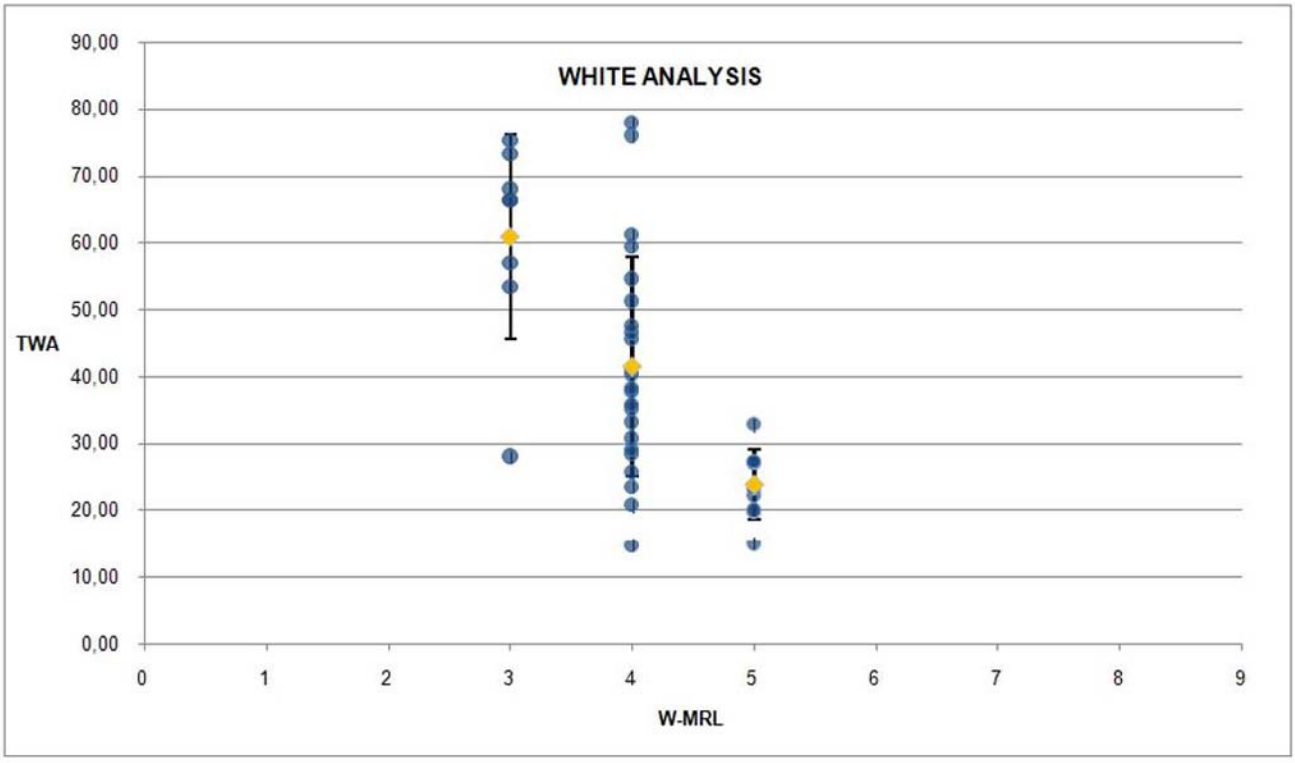
WHITE ANALYSIS
TWA
W-MRL
90,00
80,00
70,00
60,00
50,00
40,00
30,00
20,00
10,00
0,00
0
1
2
3
4
5
6
7
8
9

a

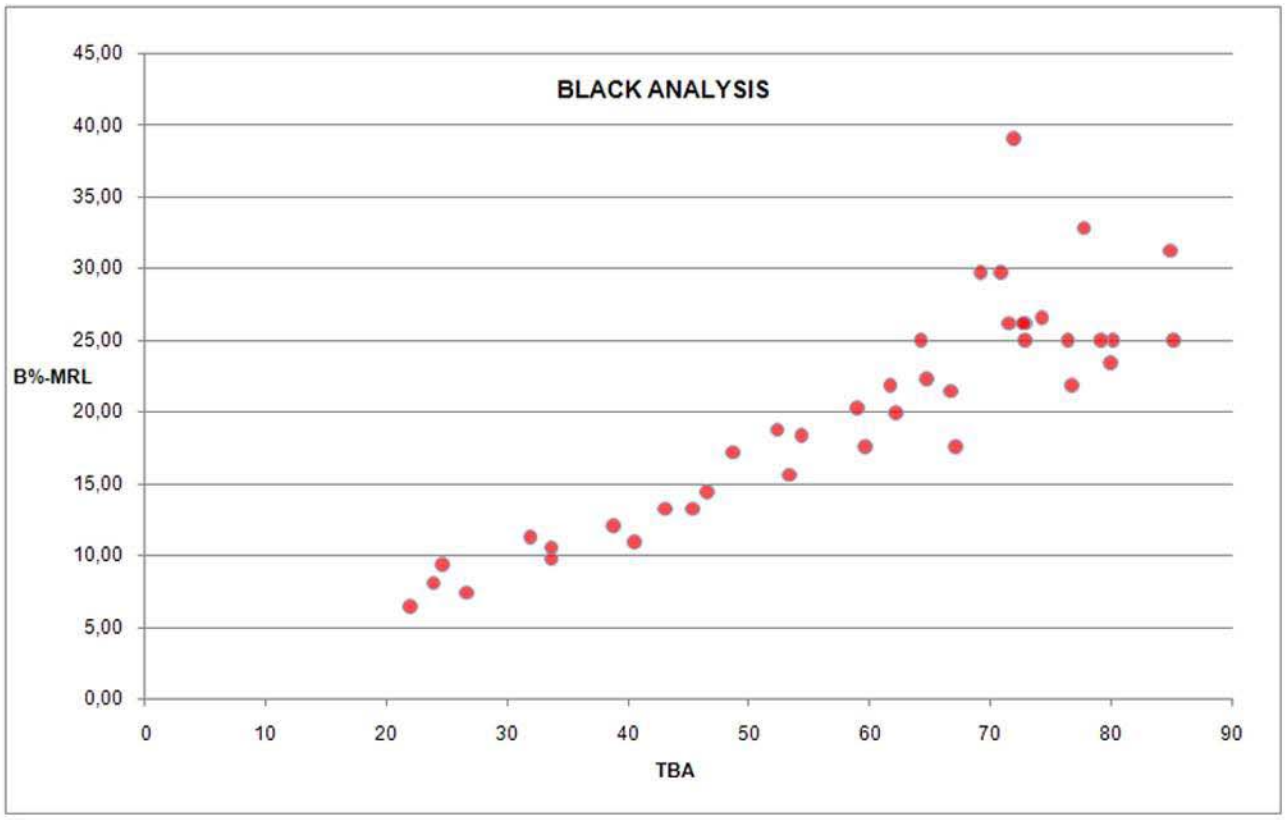
BLACK ANALYSIS
B%-MRL
TBA
45,00
40,00
35,00
30,00
25,00
20,00
15,00
10,00
5,00
0,00
0
10
20
30
40
50
60
70
80
90

b

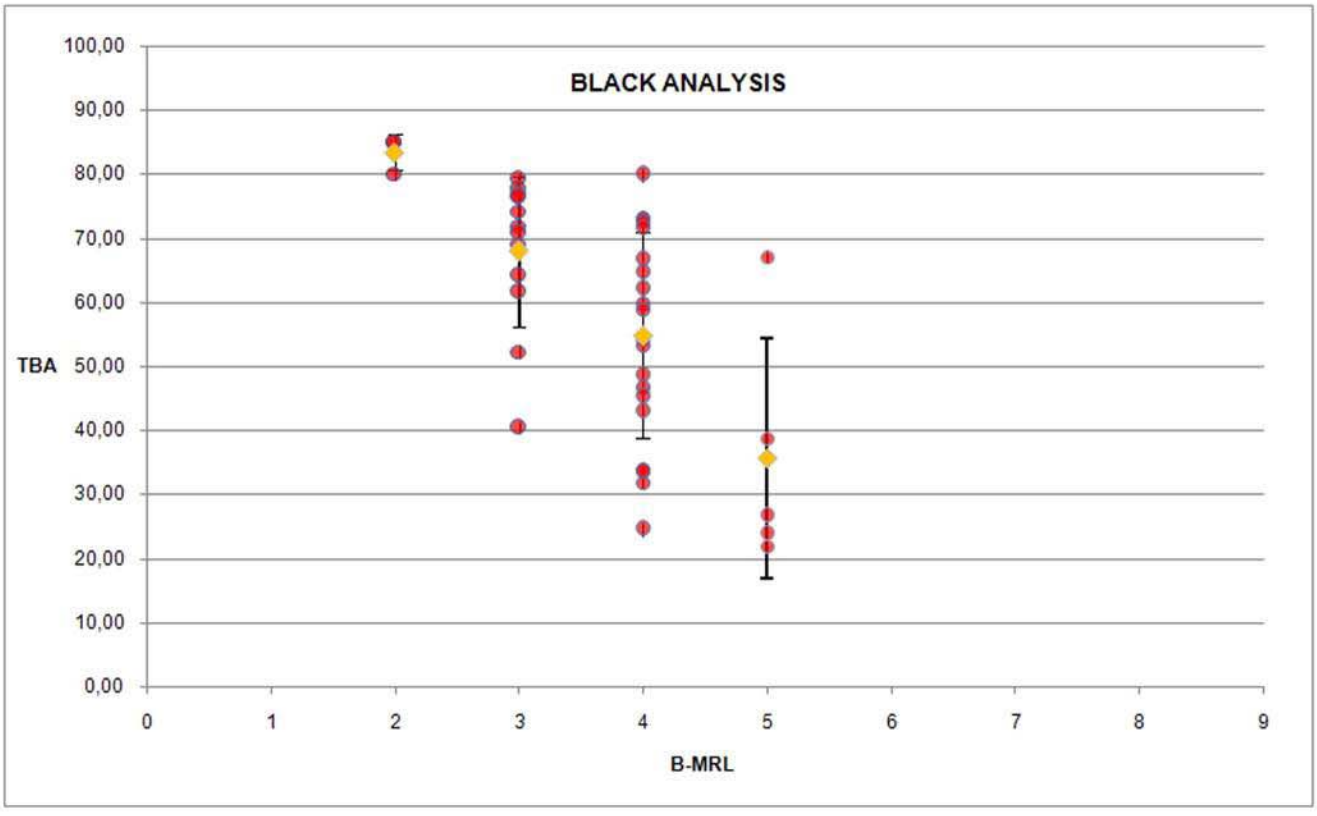
BLACK ANALYSIS
TBA
B-MRL
100,00
90,00
80,00
70,00
60,00
50,00
40,00
30,00
20,00
10,00
0,00
0
1
2
3
4
5
6
7
8
9

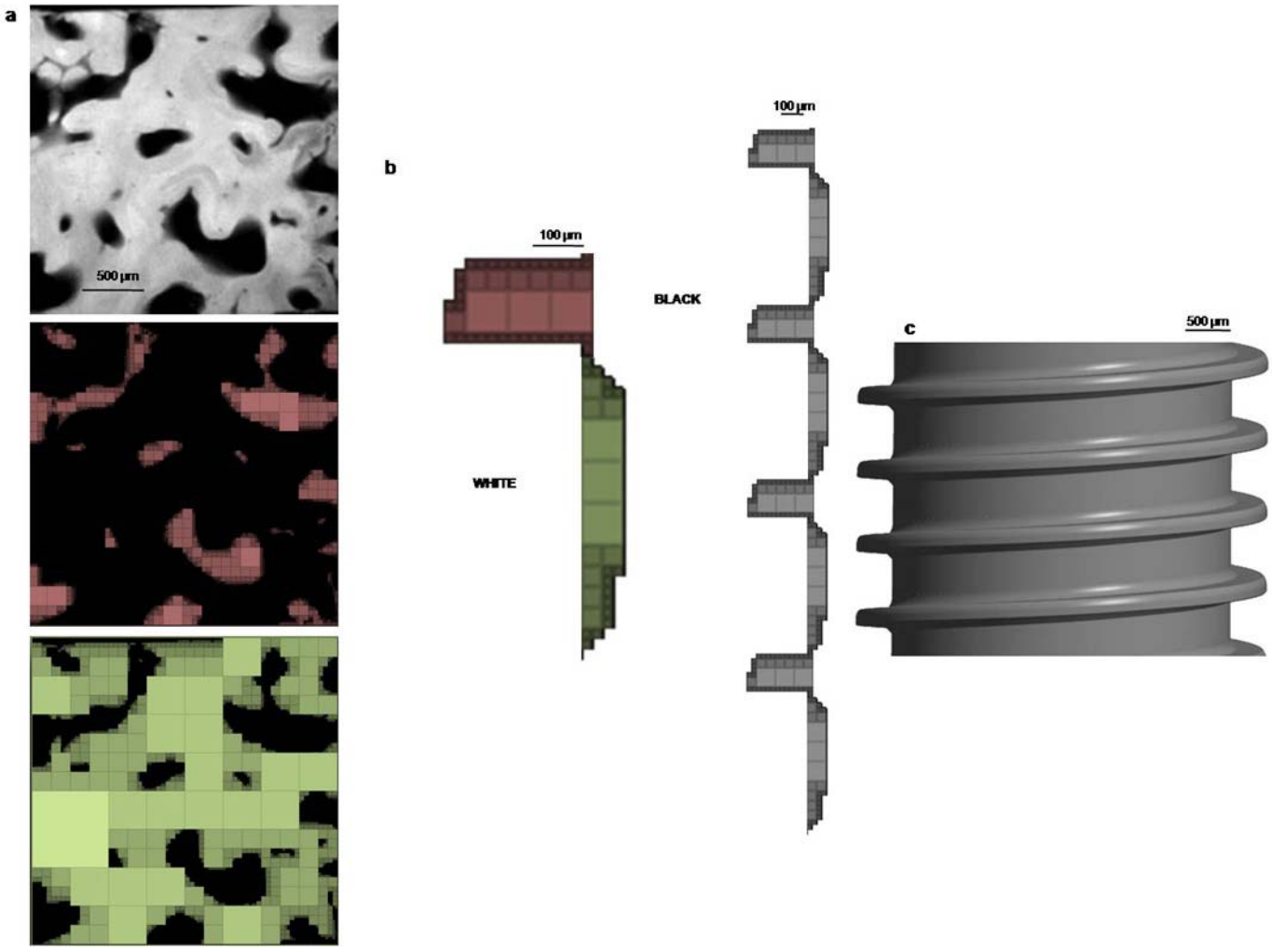
a
500 µm
b
100 µm
WHITE
BLACK
100 µm
c
500 µm

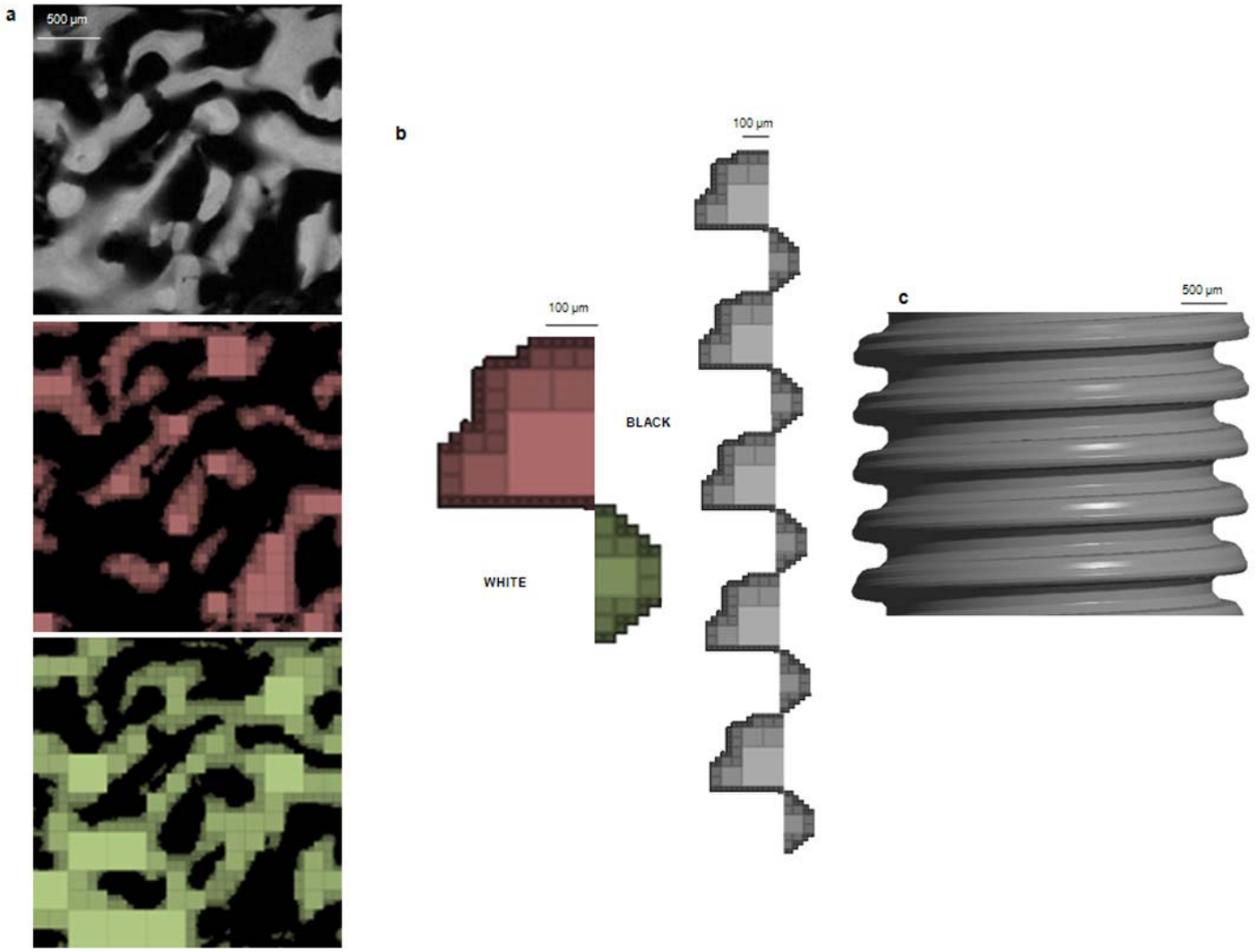
a
500 µm
b
100 µm
100 µm
BLACK
WHITE
c
500 µm

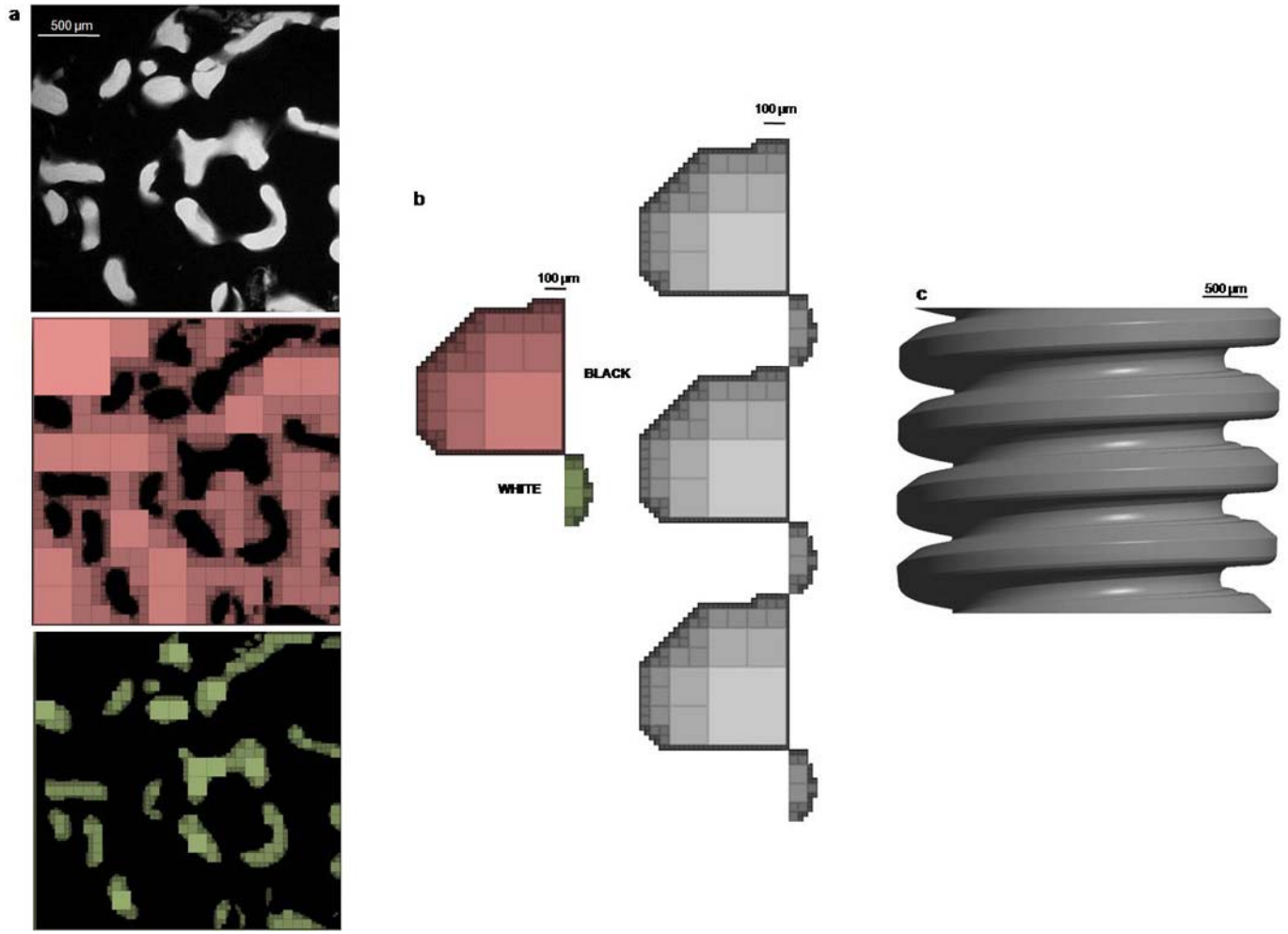
a
500 µm
b
100 µm
100 µm
BLACK
WHITE
c
500 µm